Available online at www.sciencedirect.com

SCIENCE DIRECT®

Earth and Planetary Science Letters 223 (2004) 17–34

EPSL

www.elsevier.com/locate/epsl

Serpentine and the subduction zone water cycle

Lars H. Rüpke[a,b,*], Jason Phipps Morgan[a,b], Matthias Hort[b,c], James A.D. Connolly[d]

[a] *IFM-GEOMAR, Dynamics of the Ocean Floor, Wischhofstr. 1-3, 24148 Kiel, Germany*
[b] *SFB 574, Christian-Albrechts-Universität, Kiel, Germany*
[c] *Institut für Geophysik, Universität Hamburg, Bundesstr. 55, D-20146 Hamburg, Germany*
[d] *Institut für Mineralogie und Petrographie, ETH-Zentrum, Sonneggstr. 5, CH-8082, Zürich, Switzerland*

Received 24 September 2003; received in revised form 7 April 2004; accepted 13 April 2004

Abstract

This study explores a chemo-thermo-dynamic subduction zone model that solves for slab dehydration during subduction. We investigate how changes in the incoming plate's hydration and thermal structure may effect the efficiency of sub-arc water release from sediments, crust, and serpentinized mantle. We find that serpentinized lithospheric mantle may not only be an important fluid source to trigger arc melting but is also an efficient 'transport-lithology' to recycle chemically bound water into the deeper mantle. In fact, an old slab may remain sufficiently cold during subduction to retain up to 40% of its initial 'mantle' water at 8 GPa (~ 240-km depth) after serpentine transforms to higher pressure hydrous phase A.

Furthermore, deep water recycling at subduction zones is parameterized in terms of slab age and speed. Coupling this parameterization to a parameterized mantle convection evolution model allows us to calculate the mantle-surface geologic water cycle throughout the Earth's history. We find that the present-day Earth mantle may be highly outgassed containing only a small fraction of the Earth's water, which would mostly be recycled water from the exosphere.

Keywords: subduction zone; modeling; water cycle; serpentine

1. Introduction

The subduction zone water cycle, i.e. the hydration and dehydration of subducting oceanic lithosphere, is a key process in understanding arc magmatism and volatile recycling processes. Hydration of oceanic crust begins at mid-ocean ridges through high-T and low-T hydrothermal alteration and continuing more slowly as the seafloor ages. During the plate's residence at the seafloor, sediments are continuously deposited onto it adding material containing both pore and chemically bound water. Finally, there is increasing speculation that as the plate bends during subduction, its cold lithospheric mantle may become significantly hydrated [1–4].

Dehydration occurs deeper within the subduction zone by fluid releasing metamorphic reactions. These rising fluids flux the mantle wedge where they are commonly believed to trigger arc melting (Fig. 1). It is now commonly accepted that arc lava chemistry shows a subduction component originating from the preferential transport of fluid mobile elements from the slab into the arc melting region (e.g. [5]). Like-

* Corresponding author.
E-mail address: lruepke@geomar.de (L.H. Rüpke).

0012-821X/$ - see front matter © 2004 Elsevier B.V. All rights reserved.
doi:10.1016/j.epsl.2004.04.018

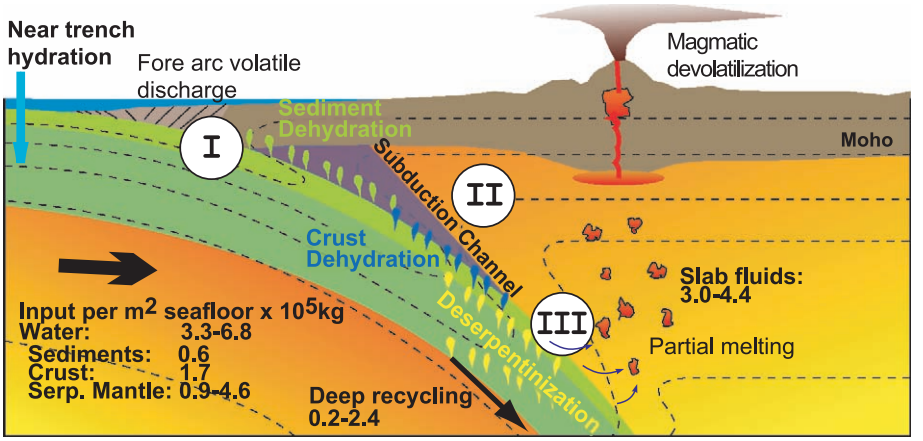

Fig. 1. Schematic drawing of the subduction zone water cycle. Water is chemically bound within the incoming plate's sedimentary, crustal, and mantle portions. Slab fluid release can be divided into three stages: (1) shallow fluid release occurs at depths <20 km from subducting sediments and may be related to fluid expulsion at cold vent sites in the fore arc region [49]. (2) Intermediate depth (20–100 km) water release from sediments and ocean crust may lead to cold upwelling along the 'subduction channel' [50]. Deep fluid release (>100 km) from oceanic crust and deserpentinizing mantle triggers arc melting. Some fraction of the incoming plate's initial water content is retained and recycled to greater mantle depths. Contour lines illustrate schematically temperatures at a subduction zone.

wise, most recent studies agree that subduction-related recycling of altered, i.e. hydrated, oceanic lithosphere is necessary to explain some aspects of the mantle's chemical evolution (e.g. [6]). Element recycling within the subduction factory is therefore intimately linked to the subduction zone water cycle.

But the subduction zone water cycle is also related to the formation and evolution of the oceans. Although the initial Earth probably accreted a large amount of exospheric water, it is likely that the moon forming impact led to the desiccation of the exosphere. After this impact, strong volcanic activity on the young Earth led to the outgassing of water from the mantle which ultimately formed the oceans (see [7] for additional information on the early Earth). It remains, however, a matter of vigorous debate how much water remained within the mantle, how much outgassed into the oceans, and how much water is potentially recycled back into the mantle at subduction zones.

A better understanding of the subduction zone water cycle therefore helps to better understand the chemical evolution of the Earth's mantle and exosphere. To further constrain this water cycle, the water input into a subduction zone and the amount of sub-arc water release both have to be known. Unfortunately, determining the water input into a subduction zone is not easy. While fairly good (and converging) estimates exist for the sediment and crustal portions of the incoming plate [8–11], much less is known about the lithospheric mantle's degree of hydration [3,4,12].

In order for surface fluids to hydrate mantle rocks, the fluids must be able to pass through the sediments and crust to reach the mantle. Normal faults occurring during plate bending between the outer rise and the trench axis provide possible fluid pathways for deep water transport. High resolution, deep imaging, seismic reflection profiles show normal faults that cut across the crust at least (>15 km) deep into the lithospheric mantle [3]. These 'bend-faults' may act as conduits for sea water to reach and react with lithospheric mantle rocks to make serpentine. In this scenario, the incoming lithospheric mantle would be highly serpentinized around these faults while the unfaulted parts would be practically dry. The average degree of serpentinization/hydration would then depend on the 'spacing' of bend-faults between the trench axis and the outer rise.

'Lithospheric' serpentine is commonly seen in Alpine peridotites, and based upon this evidence, serpentinites have previously been proposed to be a significant source of water during sub-arc slab dewatering [12,13]. Slab-mantle dehydration has also been related to double zone earthquakes [1,14–16], arc

magmatism [2], and a water-flux-forced transition from gabbro to eclogite in the subducting slab [17]. However, none of these studies can provide good estimates of the extent of downgoing lithosphere serpentinization. Serpentinites are known to have lower seismic P-wave velocities than peridotites, but as yet no good subcrustal velocity models exist save for two recent studies off Nicaragua and Chile which seem to show reduced Moho P-wave velocities between the trench axis and the outer rise [18,19] consistent with up to $\sim$ 20% near Moho serpentinization.

Unfortunately, the dehydration part of the subduction zone water cycle, i.e. the efficiency of slab dewatering through metamorphic reactions, is also quite poorly constrained. Seismic tomography, as well as geochemical studies, can provide some insights into the amount of slab derived water in the mantle wedge, but so far thermal models seem to be the most promising 'tool' for study of sub-arc water release. Here, we use a numerical model to determine a self-consistent water budget for subduction zones to help to further constrain recycling processes at convergent margins.

2. Modeling

Several previous studies have used different approaches to model the thermal and petrologic structure of subduction zones. First, Davies and Stevenson [20] and later Peacock [21] and Peacock and Wang [22] presented 'kinematic' models in which the (steady state) flow field is completely prescribed by the boundary conditions. This type of model is mainly used to map the thermal structure of specific subduction zones. To understand the dynamics of subduction, models need to include buoyancy forces, so that the flow field is time-dependent—see, e.g. [2,23–25]. Furthermore, there are 'hybrid' models that contain ingredients of both model types which are mainly used to study specific aspects of subduction that do not necessarily need a fully dynamic solution. Examples of this are studies of mantle wedge dynamics in the framework of a kinematically driven slab, e.g. [26,27].

Studies of the petrologic structure of subduction zones have so far mainly focussed on plotting calculated geotherms onto phase diagrams [21,26] (see, e.g. [28,29] for a new and thorough study). This approach is useful to generally explore which metamorphic reactions may take place during subduction but does not include any feedback mechanisms like metamorphic cooling due to latent heat consumption.

Here we present a self-consistent model for temperature, mantle flow, and water release at subduction zones. The model includes buoyancy forces but assumes a kinematically driven slab. Metamorphic reactions are self-consistently implemented using tracer particles and synthetic phase diagrams calculated with the thermodynamic tool-box PERPLEX.

2.1. Governing equations

The flow field is modeled assuming a viscous (Stoke's) flow model and the Boussinesq approximation:

$$\frac{\partial \tau_{ij}}{\partial x_j} - \frac{\partial p}{\partial x_i} - \rho g_i = 0 \tag{1}$$

$$\tau_{ij} = \mu\left(\frac{\partial u_i}{\partial x_j} + \frac{\partial u_j}{\partial x_i}\right) \tag{2}$$

$$\frac{\partial u_i}{\partial x_i} \equiv \dot{\varepsilon}_{\mathrm{v}} = 0 \tag{3}$$

Eq. (1) is the force balance, Eq. (2) the constitutive law, and Eq. (3) the incompressibility constraint. The variables are the stress tensor τ_{ij}, the pressure p, the density ρ, the gravitational attraction vector $\mathbf{g}$, the viscosity μ, the velocity vector $\mathbf{u}$, the physical coordinate vector $\mathbf{x}$, and the volumetric strain rate $\dot{\varepsilon}_{\mathrm{v}}$ (see Table 1 for a complete list of variables). Density variations only affect the buoyancy term in Eq. (1), so that:

$$\rho(T, \mathrm{dp}) = \rho_0(1 - \alpha(T - T_{\mathrm{m}}) - \beta \mathrm{dp}). \tag{4}$$

Here, T is the temperature, ρ the density and the two constants α and β are the thermal expansivity and the depletion buoyancy parameter. The depletion, dp, represents the total amount of melt extraction experienced by a parcel of mantle. Although we do not solve for melting in our model, we use this parameter to account for compositional density dif-

Table 1
Complete list of symbols and parameters used in the model formulation

Symbol	Meaning	Value	Dimension
A	average sea floor age	–	Ma
A_{ocean}	average area of oceans	–	m^2
H_{wr}	heat of water release	–	K
J	Jacobi matrix	–	–
L	latent heat	–	J kg^{-1}
P_0	present fraction of mantle processed at ridges per year	1.0527×10^{-10}	$year^{-1}$
R	overturn rate of the Earth's mantle	–	–
R_0	present overturn rate of the Earth's mantle	9.5	Ga
S_0	present-day average spreading rate	2.7×10^6	m^2/year
T	temperature	–	K
T^*	dimensionless temperature	–	–
T_m	basal asthenosphere temperature	1573	K
T_0	surface temperature	273	K
V	total volume of water in the exosphere	–	m^3
b	temperature dependence of viscosity	15	–
c_p	specific heat	1250	J kg^{-1} K^{-1}
d	ocean depth	–	m
dp	depletion	0–0.4	–
f_{H_2O}	volatile outgassing efficiency during melting	0.99	–
g	gravitational acceleration	9.81	m s^{-2}
h	change in sea level	–	m
n	time stepping index	–	–
p	pressure	–	Pa
t	time	–	s
u_0	convergence rate	6.0	cm/year
$\mathbf{u}(u,w)$	velocity vector	–	m s^{-1}
$\mathbf{x}(x,z)$	coordinate vector	–	m
α	thermal expansion constant	3×10^{-5}	K^{-1}
β	comp. buoyancy parameter	0.5×10^{-2}	–
$\dot{\varepsilon}$	volumetric strain rate	–	–
κ	thermal diffusivity	10^{-6}	m^2/s
ρ	density	–	kg m^{-3}
ρ_0	reference mantle density	3300	kg m^{-3}
μ	viscosity	–	Pa s
μ_0	reference viscosity	10^{19}	Pa s
ϕ	degree of hydration	0–1	–
τ_{ij}	stress tensor	–	–
$\boldsymbol{\xi}$	logical tracer coordinate vector	–	–

ferences within the slab and among the incoming and overriding plate.

As a cautious note, we want to emphasize that although we account for buoyancy in the model formulation, the intra-slab flow field is almost entirely prescribed by the boundary conditions since we assume a kinematically driven slab (see section on boundary conditions). Although this is a simplification that prevents us from correctly treating the dynamics of subduction, we chose to prescribe the slab in order to be able to explore for a wide parameter range the effects of different incoming plate ages and speeds on the thermal solution without having to carefully adjust for every model run the viscous and buoyancy forces to match a certain subduction rate.

Furthermore, we use a simple temperature-dependent Newtonian viscosity law and augment it with a pressure dependence that crudely simulates an increase in 'deeper mantle' viscosity beneath 450 km:

$$\mu(T,z) = \mu_0 \mu(z) \exp\left[b\left(\frac{1}{T^*} - 1\right)\right] \tag{5}$$

$$\mu(z) = 1 + [(250-1)/2][1 + \tanh(0.01(z-450))]; \tag{6}$$

b is a parameter characterizing the temperature dependence of viscosity [30] and $T^* = T/T_m$ is the dimensionless viscosity. Note that we do not explicitly account for phase changes at the 410- and 660-km discontinuity. Once the flow field is known, the advection diffusion equation for temperature can be solved. Here, we use a formulation of the heat transport equation that includes the latent heat effect of metamorphic reactions, i.e. the cooling of the subducting slab due to its devolatilization:

$$\frac{\partial T}{\partial t} + \left(u\frac{\partial T}{\partial x} + w\frac{\partial T}{\partial z}\right) - \kappa\left(\frac{\partial^2 T}{\partial x^2} + \frac{\partial^2 T}{\partial z^2}\right) + H_{wr}\frac{\partial \phi}{\partial t} = 0 \tag{7}$$

Here, u, w, x, and z are the horizontal and vertical velocity and distance components. H_{wr} is a latent heat term ($H_{wr} = L/c_p$) and ϕ is the weight fraction of chemically bound water. In our model calculation,

we do not include hydration processes, but rather prescribe an initial hydration of the incoming plate. As the subducting plate dewaters, we assume that the liberated water 'leaves' the system, so that no new hydrous phases are formed during subduction. This implies that the term $\partial\phi/\partial t$ is always less or equal to zero.

2.2. Solving the equations

We use a combined finite element-finite difference technique to solve for mantle flow and temperature. For the mantle flow part, we discretize the modeling domain into rectangular four velocity node-constant pressure finite elements, and use the penalty method to solve the flow equations. To solve the advection–diffusion equation, we use the high precision finite differences algorithm MPDATA which has relatively small numerical diffusion problems [31]. Since the heat transport equation includes a source term that accounts for metamorphic cooling, we iterate to obtain a self-consistent temperature solution.

2.3. A tracer based model for slab petrology

We use a tracer particle advection scheme to track the subducting slab's chemical evolution. Tracer advection schemes have the advantage that they do not suffer from numerical diffusion, so that they are well suited for advecting non-diffusive properties like chemically bound water. First, we present the tracer method. Second, we will apply it to the specific problem of tracking chemically bound water during the subduction water cycle.

Standard tracer advection algorithms consist of four parts: the advection equation (Eq. (8)), an integration scheme, a localization process, and the Jacobi matrix determinations [32]. A tracer's position is determined by its cell number and location, and can be expressed in physical, $\mathbf{x}$ or logical coordinates, $\boldsymbol{\xi}(0<\xi_i<1,\ \text{with}\ i=x,z)$. The logical and physical coordinates are interconnected by the Jacobi matrix, $\mathbf{J}$, so that $\boldsymbol{\xi}=\mathbf{J}^{-1}\mathbf{x}$. Logical coordinates have the advantage that whenever a logical coordinate is unbound after integration (i.e. $\xi_i<0$ or $\xi_i>1$), a tracer particle has changed cells and a localization process is necessary.

The tracer advection scheme can be written as:

$$\frac{\partial\bar{\xi}}{\partial t}=\left[\frac{\partial\mathbf{x}(\xi)}{\partial\xi}\right]^{-1}\cdot\mathbf{u}_x(\mathbf{x}(\xi,\mathbf{t}))=\mathbf{u}_\xi(\mathbf{x}(\xi,\mathbf{t})) \tag{8}$$

$$\bar{\xi}^{n+\frac{1}{2}}=\bar{\xi}^{n}+\mathbf{u}^{n}\cdot\frac{\Delta t}{2} \tag{9}$$

$$\bar{\xi}^{n+1}=\bar{\xi}^{n}+\mathbf{u}^{n+\frac{1}{2}}\cdot\Delta t \tag{10}$$

where $\mathbf{u}_x$ is the physical coordinate velocity vector and $\mathbf{u}_\xi$ the logical coordinate velocity vector; n is the time stepping index and t the time. The integration scheme always contains a trade-off between speed and accuracy. A simple Eulerian integration scheme requires only one evaluation of the RHS of Eq. (8), but often critically reduces accuracy. We use a predictor–corrector advection scheme (Eqs. (9) and (10)) that requires two evaluations of the RHS of the advection equation per time step but provides the required level of accuracy. Higher order integration schemes appeared to unnecessarily increase the computational costs without a noticeable change in particle tracking in the downgoing slab. The localization method is straightforward since we use a structured orthogonal grid.

To model metamorphic reactions, we treat each tracer as an object that contains in addition to its location and cell number also density, volume, water content, and thermal enthalpy. These properties are mapped and scaled onto the grid points (i.e. the cell nodes) using the finite element shape functions and each tracer's volume. The change in tracer properties during subduction is determined with look-up tables pre-calculated with the thermodynamic tool-box PERPLEX [33]. PERPLEX allows the calculation of $p-T$ property plots for any constrained bulk composition.

2.4. Initial and boundary conditions

We solve the equation within a (1600×800 km) sized rectangular box (Fig. 2). To enhance the resolution within the region of interest, we use an asymmetric mesh ($\sim$ 21 000 nodes) with a maximum grid resolution of 2 km in the subduction 'hinge-region'. For boundary conditions, we assume: on the left-hand side of the box the horizontal velocity decreases linearly from the convergence rate at the top to zero at the bottom of the box—temperature is held constant

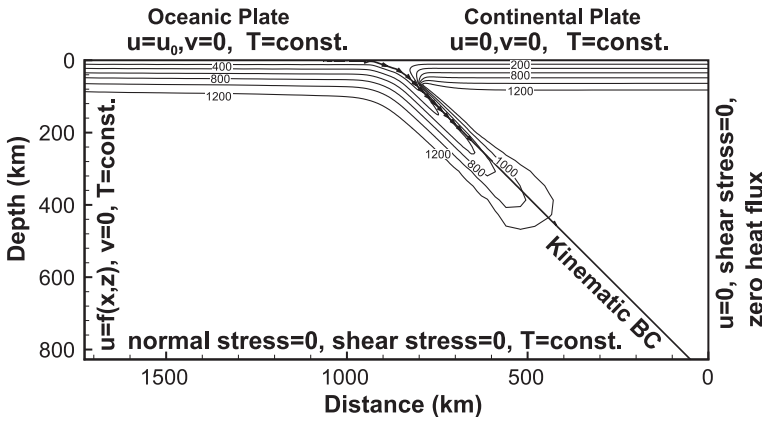

Fig. 2. The modeling domain. We use a asymmetric mesh with a maximum resolution of 2 km in the regions of slab dewatering.

at its initial value; the bottom of the region is assumed to be stress-free and the temperature is constant; the right-hand side of the region is a symmetry plane with zero heat flux across it; the top surface has zero vertical velocity with the horizontal velocity of the overriding plate set to zero; the horizontal velocity of the incoming plate equals the convergence rate, u_0, and the temperature is constant. We initialize the temperature field using a simple half-space model for oceanic lithosphere for the incoming plate and a continental geotherm for the overriding plate that corresponds to 70 mW/m^2 surface heat flux [34]. We set the depletion by assuming that the degree of depletion rises linearly from 0% at a depth of 70 km to 20% at the top of the incoming plate (this would be depletion due to MOR melt extraction) and from 0% at a depth of 70 km to 30% at the top of the overriding, continental plate. To decouple the motion of the overriding plate from the subducting plate, we prescribe "weak nodes" along the trench according to the initial slab dip [23]. To isolate the effects of plate age and speed on slab dehydration (and exclude the potential impact of differing dip angles), we set the velocities at the slab surface to a prescribed value. This modification results in a more kinematically driven slab that subducts with constant dip (45°) and speed.

3. Water cycling beneath an arc

Water cycling beneath an arc depends on: (1) the incoming plate's initial hydration, (2) the amount of water release from the slab, and (3) the degree of water recycling into the deeper mantle. Water release and water retention depend upon the metamorphic reactions that occur during subduction and slab metamorphism is controlled by the thermal regime of subduction. We shall therefore first discuss the thermal solution of our model.

3.1. Sensitivity of the thermal solution to subduction parameters

In this study we explore how changes in subduction parameters (plate age and speed) may effect the thermal structure and thereby water release beneath an arc. Fig. (3a–c) shows calculated p–T paths for different incoming plate ages and subduction rates. All solid lines refer to the slab surface and the dashed lines to p–T conditions 8 km beneath the slab surface within the uppermost lithospheric mantle. It is clear that for all convergence rates, temperatures within the slab are generally higher when young/hot seafloor is subducted. Differences in subduction rate do, however, influence the thermal solution in that slower subduction rates lead to hotter geotherms because the slab has more time to heat up by conduction.

Slab surface temperatures show in all cases a typical S-shaped form when plotted against depth: at depths <70 km the geothermal gradient is low and the heating of the slab is dominated by heat conduction from the upper plate. At depths >70 km, the slab surface is exposed to the hot convecting mantle wedge. Wedge convection leads to a steady flow of

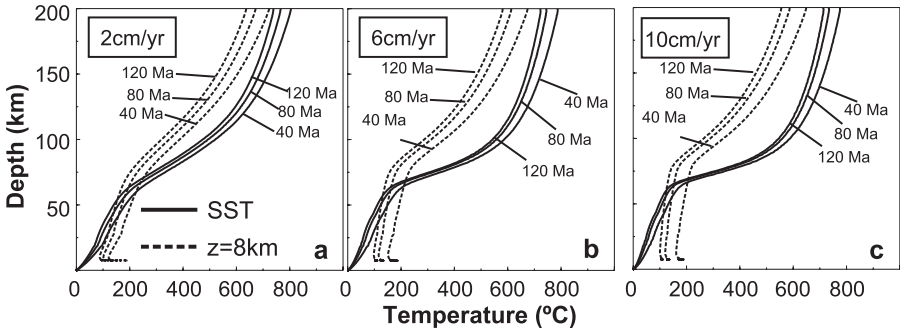

Fig. 3. Sensitivity of geotherms on subduction parameters. Solid lines show slab surface temperatures and dashed lines temperatures within the lithospheric mantle 8 km below the slab surface.

hot mantle material towards the slab which rapidly heats the slab surface and gives rise to a steeper geothermal gradient. Once the slab surface has heated up closer to mantle wedge temperatures, the geothermal gradient flattens again. However, the higher the subduction rate, the more pronounced the S-shape form of a geotherm. This results from the vigor of convection in the mantle wedge: the higher the subduction rate, the more vigorous is wedge convection with resultant stronger heating of the slab surface.

Temperatures within the subducted lithospheric mantle are not so affected by mantle wedge convection, since conduction is too sluggish to rapidly transport heat from the slab surface to the lower crust and upper mantle. Upper slab mantle geotherms therefore show a less pronounced S-shaped form. The slab surface therefore heats up much more rapidly due to heating from the mantle wedge while the deeper parts of the slab may remain significantly colder during subduction leading to an inverted temperature profile.

These results are qualitatively and quantitatively close to the results of similar previous models: van Keken et al. [26] found the same effects of wedge convection on slab surface temperature and when compared to Peacock and Wang [22] estimates for 'hot' and 'cold' subduction, our geotherms represent intermediate to cold subduction temperatures. None of our geotherms comes close to 'hot' subduction because we neglect shear heating. We believe that high shear stresses are unlikely to occur within the fault zone; the feedback between shear heating and frictional strength will lead to a reduced strength of the décollement before significant heating can occur. Since the amount of shear heating is largely unconstrained, we have neglected its effects in these calculations. However, the good fit with previous models lets us believe that our thermal solution is stable and realistic.

Another geodynamic parameter we neglect but which may affect the thermal solution is the dip angle. The justification of this simplification is that the main application of this model is to calculate water recycling at paleo-subduction zones. While we get information on slab age and speed from a parameterized convection model (see Section 5), no information is available for dip angle. For this reason, we use a constant dip angle in all model runs. Note that steeper dip angles usually result in slightly colder geotherms, since conduction has less time to heat up the slab.

3.2. The incoming plate composition and hydration

Plank and Langmuir [8] defined an average composition of marine sediments (GLOSS). GLOSS contains 7.29 wt.% water and in our model runs we assume a sediment thickness of 350 m. These values result in a water content of 0.6×10^5 kg/m^2 in a column of sediment. Average ocean crust has a thickness of 6 km and is only partially hydrated (see Fig. 4a). We make a conservative estimate of the average hydration of oceanic crust by assuming that top first kilometer is highly altered and contains 2.7 wt.% water. This highly altered layer is underlain by a less hydrated (1 wt.% water) 2-km-thick layer. The gabbroic lower portions are assumed to be anhydrous. This composition corresponds to a water content of 1.7×10^5 kg/m^2 in a crustal column. In this study, we center on the role of serpentinized mantle for water cycling at convergent margins. Unfortunately, the oceanic lithospheric man-

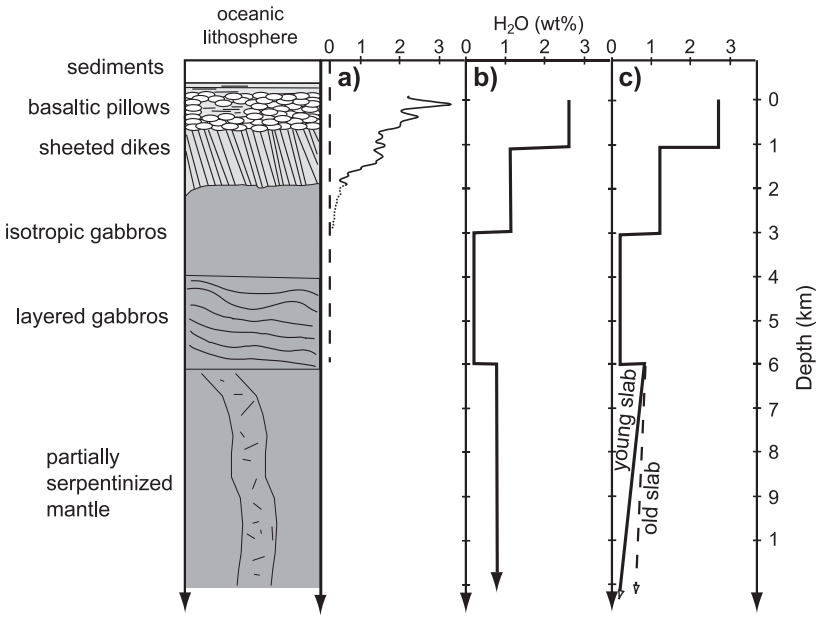

Fig. 4. Three different possible models illustrating the degree of hydration of typical oceanic lithosphere. The curve in (a) is based on literature values on the degree of hydration of oceanic crust. In (b) the incoming oceanic lithosphere includes a 10-km-thick partially serpentinized mantle layer. Our preferred model is shown in (c) we assume that the degree of lithospheric mantle serpentinization decreases linearly from 5% at the Moho to zero at the depth and temperature where serpentine becomes unstable (~ 600 °C). This model implies that old slabs contain more water bound in serpentine than young slabs.

tle's hydration is not well constrained. In our initial model runs, we will assume that the incoming lithosphere contains a 10-km-thick weakly (5%) serpentinized mantle layer (2.0×10^5 kg/m^2) of water. Fig. 4b illustrates this initial plate composition.

We use the PERPLEX tool-box to calculate the necessary phase diagrams and $p-T$ property plots for hydrated sediments, crust, and mantle (Fig. 5). In a,b the phase diagram and $p-T$ water content for GLOSS is shown (for a more detailed discussion of the phase relations, see [10]). For altered oceanic crust, we use Staudigel's (1996) [9] composition for metabasalt and c,d show the calculated phase relations and $p-T$ water content—see [35] for a more detailed discussion of the phase relations. As an initial composition of hydrated mantle, we use the one for harzburgite given in [12] and the computed phase relations are shown in Fig. (5e).

3.3. Sub-arc water release

We have made two example model runs assuming a young (40 Ma) slab and an old (120 Ma) slab to explore where fluids are released from a subducting plate. For these two cases, Fig. 6a and b shows the temperature field together with the regions of water release: green contour lines mark sediment dewatering, cyan contour lines water release from the crust, and yellow contour lines mantle deserpentinization, and c,d show the relative amount of water retention with depth.

The modeled pattern of water release from an 40-Ma-old slab, shown in Fig. 6a, resembles the sche-

Fig. 5. Computed phase equilibria and $p-T$ water content plots for the three different slab fluid sources GLOSS sediments, metabasalt, and serpentinized mantle. Mineral abbreviations are: A-phase; 'phase A'; Anth, anthophyllite; Atg, antigorite; B, brucite; Bio, biotite; Chl, chlorite; coe, coesite; Cpx, clinopyroxene; cz, clinozoisite; Gln, glaucophane; Grt, garnet; Lws, lawsonite; Opx, orthopyroxene; q, quartz; T, talc; stv, stishovite. Some mineral phases that are present in all fields have been omitted in the labelling: for GLOSS these are phengite, quartz/coesite, and fluid; for metabasalt, clinopyroxene and phengite; and for hydrous peridotite, olivine and clinopyroxene. Additionally, geotherms at different positions within 40- and 120-Ma-old subducting lithosphere are shown.

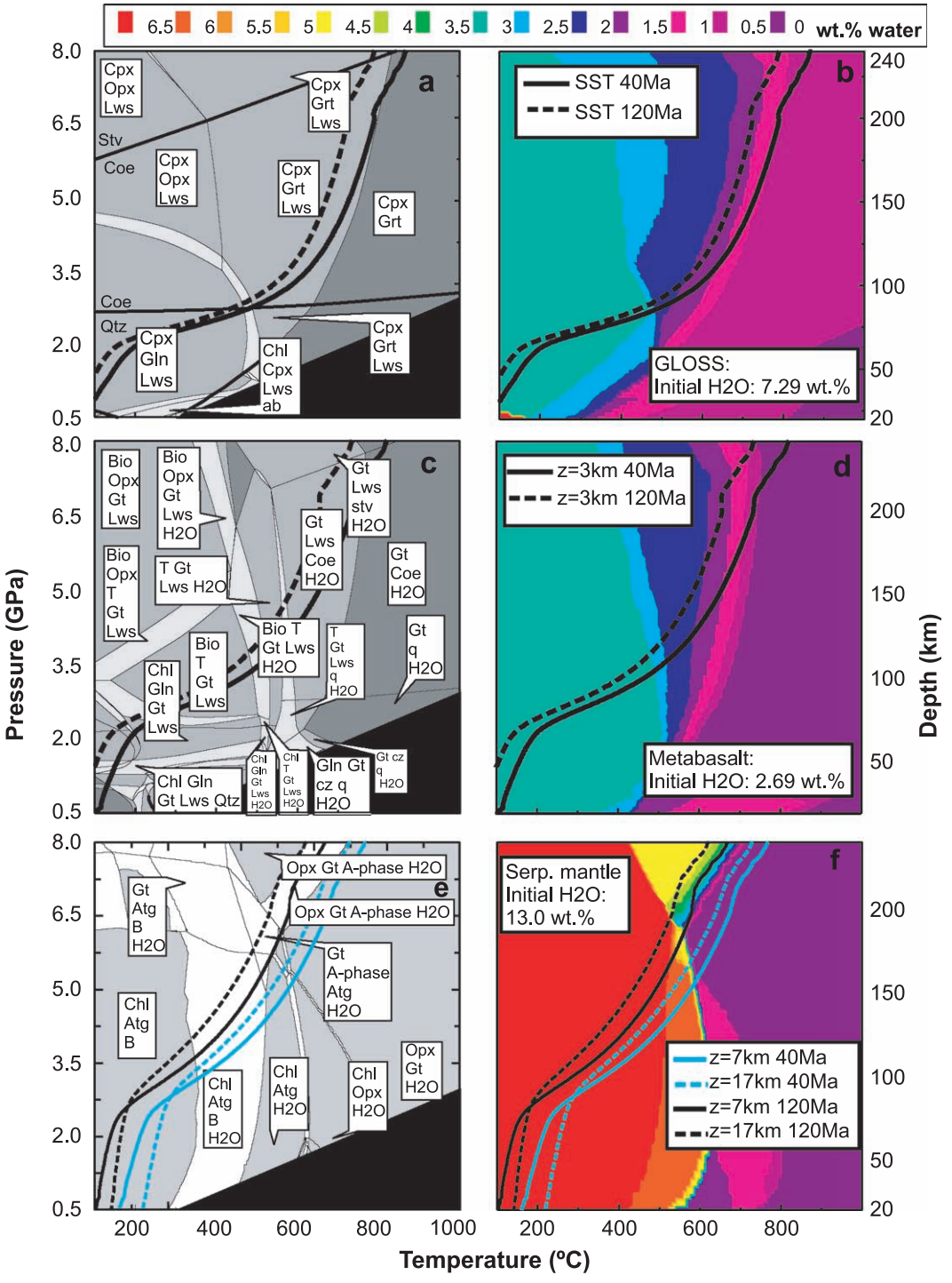
6.5 6 5.5 5 4.5 4 3.5 3 2.5 2 1.5 1 0.5 0 wt.% water
a
Cpx Opx Lws
Cpx Grt Lws
Stv
Coe
Cpx Opx Lws
Cpx Grt Lws
Cpx Grt
Coe
Qtz
Cpx Gln Lws
Chl Cpx Lws ab
Cpx Grt Lws
b
SST 40Ma
SST 120Ma
GLOSS:
Initial H2O: 7.29 wt.%
c
Bio Opx Gt Lws
Bio Opx Gt Lws H2O
Gt Lws stv H2O
Gt Lws Coe H2O
Gt Coe H2O
Bio Opx T Gt Lws
T Gt Lws H2O
Bio T Gt Lws H2O
T Gt Lws q H2O
Gt q H2O
Bio T Gt Lws
Chl Gln Gt Lws
Chl Gln Gt Lws H2O
Chl T Gt Lws H2O
Gln Gt cz q H2O
Gt cz q H2O
Chl Gln Gt Lws Qtz
d
z=3km 40Ma
z=3km 120Ma
Metabasalt:
Initial H2O: 2.69 wt.%
e
Opx Gt A-phase H2O
Opx Gt A-phase H2O
Gt Atg B H2O
Gt A-phase Atg H2O
Chl Atg B
Chl Atg B H2O
Chl Atg H2O
Chl Opx H2O
Opx Gt H2O
f
Serp. mantle
Initial H2O:
13.0 wt.%
z=7km 40Ma
z=17km 40Ma
z=7km 120Ma
z=17km 120Ma
Pressure (GPa)
Depth (km)
Temperature (ºC)
8.0
6.5
5.0
3.5
2.0
0.5
240
200
150
100
50
20
200 400 600 800 1000
200 400 600 800

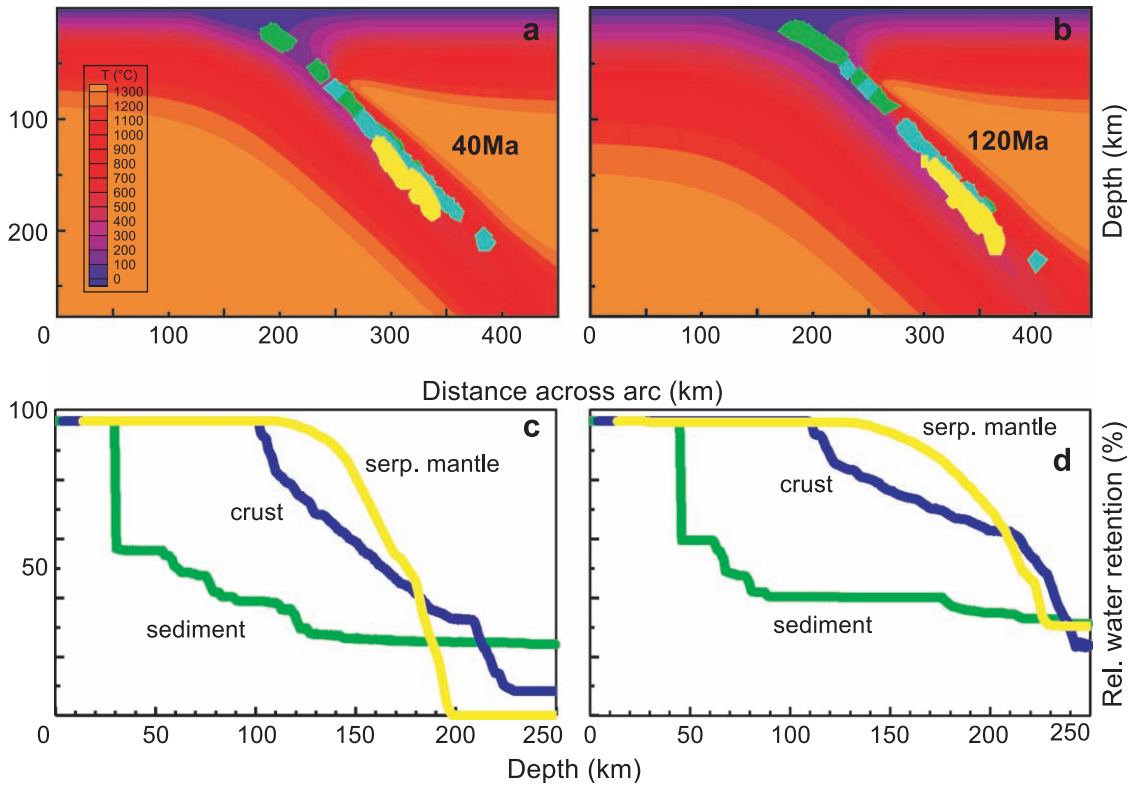

Fig. 6. Modeled water release at a subduction zone. In (a) and (b), the modeled regions of water release from subducting sediments (green), oceanic crust (cyan), and serpentinized mantle (yellow) are shown for 40- and 120-Ma-old slabs, respectively. (b) and (c) show the relative degrees of water retention at 8 GPa for the three different lithologies.

matic scenario in Fig. 1. Water is continuously released from the subducting slab with the host reservoir changing with depth. Sediments start to dehydrate at shallow depths, at ~ 50-km depth the sediments have already dewatered to over 50%, and by ~ 100 km they contain only ~ 25% of their initial water chemically bound in residual lawsonite. The reason for the shallow dehydration is twofold: (1) the slab surface is the hottest part of the slab and (2) GLOSS contains initially a lot of water that can only be chemically stored at low pressures and temperatures. Oceanic crust efficiently (~ 92%) dewaters between ~ 100- and ~ 200-km depth. The relatively deep dewatering of oceanic crust may partially result from the low initial water content: at low pressures and temperatures, metamorphic reactions (e.g. chlorite and glaucophane breakdown) appear to be water conserving, so that dewatering does not start until the crust has heated up to approximately 550 °C.

Deep water recycling is controlled by the stability of lawsonite which is the main water carrier at higher pressures. Dehydration of serpentinized mantle occurs between 120- and 200-km depth. When looking at the $p-T$ paths plotted onto the phase diagram of hydrous peridotite in Fig. (5e and f), it is clear that temperatures within the entire hydrated mantle layer exceed the stability field of serpentine before 'phase A' can form, so that all water is released.

Comparing these results to the modeled pattern of water release from an older (120 Ma) slab, (Fig. 6b and d) shows that the general pattern persists, so that first sediments, then crust and finally mantle dehydrates. The exact depths of water release do, however, change with the incoming plate's age; subduction of an older plate leads to colder geotherms (Fig. 3), so that fluid release from an older slab is less efficient and occurs at greater depths. Within a 120-Ma-old slab, oceanic crust may retain ~ 23% of its initial

water, and serpentinized mantle may retain even more water (~ 35%). This efficient potential water retention in hydrous peridotites results from the altered thermal structure of the hydrated mantle layer: parts of this layer may remain cold enough (<600 °C) for serpentine to transform to higher pressure 'phase A' thereby retaining some water to be recycled into the deeper mantle (Fig. 5e and f). It is clear that the total dehydration efficiency decreases with increasing incoming plate age: ~ 95% for a 40-Ma-old slab and ~ 71% for a 120-Ma-old slab.

These findings depend strongly, of course, on the validity of the computed phase relations. Especially deep water recycling in sediments and crust is strongly dependent on the accuracy of the calculated phase relations for lawsonite. To minimize potential errors, we have carefully checked the calculated stability field of lawsonite with experimental data [12] and find very good agreement. Deep water recycling in hydrated peridotites depends mainly on the reaction curve serpentine → phase A. Ambiguous experimental data exist for this reaction and we will discuss the synthetic phase relations we used in the next section.

4. Deep water recycling

We have shown that some fraction of a slab's initial water content may still be chemically bound at 8 GPa (~ 240 km). While a small fraction of this water is likely to be bound in subducting sediments and oceanic crust, we will show that deep water recycling may easily be dominated by subducting hydrated lithospheric mantle, so that we here focus on the role of serpentine. But what happens to chemical water that 'survives' the primary stages of sub-arc dewatering? It is a vigorous topic of current research if and how slabs can recycle water into the transition zone or the deeper mantle [36–38]—see [39] for a review of water in the Earth's upper mantle. For water to be transported into the deeper mantle, an uninterrupted chain of hydrous minerals has to be stable towards higher pressures and temperatures. Up to pressures of ~ 6 GPa and temperatures of ~ 600 °C, serpentine is the dominant water carrier in hydrated mantle rocks. Above this 'choke point' the most likely water carrier minerals are the dense hydrous magnesium silicates (DHMS) (e.g. [36]). Of the DHMS, phase A is probably the only mineral stable at sufficiently low pressures and temperatures to form by the consumption of water liberated from the breakdown of serpentine. Mapping the stability field of phase A is, however, experimentally difficult and this stability field varies from study to study [40,41]. The situation is further complicated by the fact that most experimental studies use the simplified $MgO–SiO_2–H_2O$ (MSH) system. In this aluminum and iron free reference system, the stability field of phase A is maximum. For more complicated/realistic compositions little data is available. To address this problem, we have modeled iron-solution in brucite, antigorite, and phase A by making the assumption that the enthalpic effect of octahedral iron substitution in these minerals is identical to that in chlorite as evaluated from the data of Holland and Powel [42]. This results in a reduced stability field of phase-A and the computed phase relations are shown in Fig. 5e. In our model runs we explore deep water recycling by studying how much water is still chemically bound at 240-km depth. This value is the maximum amount of water that may be transported into the deeper mantle.

4.1. The role of plate age and speed

The results presented in Section 3 have shown that the incoming plate's age affects the efficiency of fluid release during subduction. These calculations assumed a constant, i.e. age-independent, initial plate composition. However, the thermal structure of the incoming plate may also affect its initial hydration. In our initial model runs, we assumed a serpentinized mantle layer of constant thickness (10 km). This thickness, however, is not consistent with the offset (up to 50 km) between the upper and lower plane earthquakes in slabs that have double plane earthquakes. It has been previously speculated that the lower plane earthquakes may be triggered by serpentine dehydration [1,14,15]. This would, however, suggest that sea water circulation and therefore serpentinization may occur at depths of up to 50 km within the bending plate. This might imply that maybe it is not the maximum penetration depth of sea water that is the depth limiting factor for slab serpentinization, but rather the fact that at a certain depth the slab simply becomes too hot (>600 °C) to make serpentine. If the ~ 600 °C isotherm marks the maximum

depth to which lithospheric mantle rocks may become hydrated, this implies that old plates may contain more water than young plates because the depth of this isotherm is plate age-dependent. We therefore speculate that a more likely incoming plate composition could include a hydrated mantle that is 5% serpentinized at the crust mantle boundary but the degree of serpentinization decreases linearly from an average of 5% at the Moho to 0% where serpentine becomes unstable (~ 600 °C) (Fig. 4c). Remember that these average values represent the 'spacing' of fully hydrated faults. Our incoming plate composition therefore implies that the number of hydrated faults reaching a given depth decreases linearly from the Moho with depth. In this scenario a column of serpentinized mantle of a young (20 Ma) slab contains 0.9×10^5 kg/m^2 of water and an old (160 Ma) slab contains 4.5×10^5 kg/m^2.

Fig. 7 shows the outcome of a series of model runs in which we systematically vary the incoming plate's age and hydration. In (a) the total amount of subducted water is plotted, in (b) the relative water retention at 8 GPa is shown, in (c) the absolute water retention, and in (d) the absolute amount of sub-arc

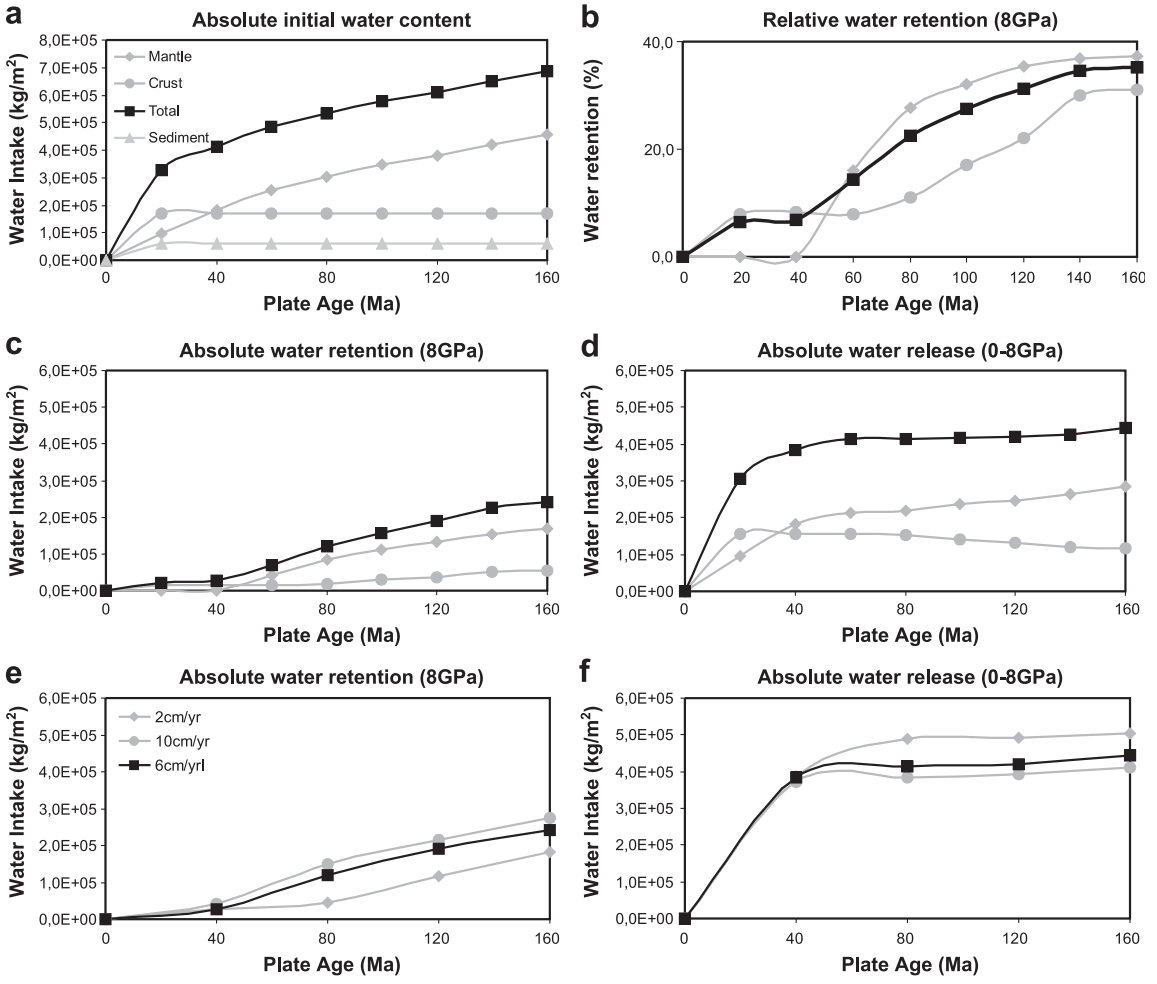

Fig. 7. Water intake, release, and retention of a subducting slab for varying plate ages. (a) Shows the amount of subducting chemically bound water, (b) shows the relative water retention at 8 GPa (~ 240-km depth), (c) the absolute amount of water retention, and (d) the amount of water release into the arc melting region. In (e) and (f) the total amount of sub arc water release and water retention at 8 GPa is shown for different convergence rates.

water release as a function of incoming plate age. A closer look at the water retention at 8 GPa shows that older slabs do not only contain more water (a), they also remain sufficiently cold during subduction to retain relatively more water than younger slabs (b) and thereby recycle also more water in absolute values to greater mantle depths (c). It is clear from the relative (b) and absolute (c) water retention at 8 GPa that the amount of deep water recycling can easily be dominated by water retention within the subducting plate's serpentinized mantle layer. Lithospheric serpentinites may retain up to ~40% of their initial water content (160-Ma-old slab; 10 cm/year) and are therefore the most stable lithology to transfer chemically bound water beneath the primary depths of sub-arc water release into the deeper mantle. Note that water retention within the basaltic crust also increases with increasing plate age, so that a 160-Ma-old, rapidly subducting (10 cm/year) slab may retain ~35% of its initial crustal water.

It is clear from Fig. 7a that oceanic sediments do not contain enough water to significantly influence the subduction zone water cycle. We have therefore for clarity not explicitly plotted the results for sediments in (b–d); the sediment contribution is, however, included in the total values plotted in (b–f). In (d) the total amount of water release into the sub-arc melting region is shown. In contrast to water retention, sub-arc water release does not correlate with the total amount of subducted water. In fact, the amount of water release remains remarkably constant for differing plate ages/hydrations.

Another geodynamic parameter that may directly influence fluid release from a subducting slab is the convergence rate or plate speed. To constrain how differing plate speeds affect fluid release, we have performed the same set of model runs with varying subduction rates. Plots (e) and (f) show the total amount of water retention and sub-arc water release for plates subducting at 2 and 10 cm/year, respectively. These model runs show that higher subduction rates lead to 'colder' slabs and thereby less sub-arc water release.

5. The geologic water cycle

So far we have discussed water cycling beneath an arc only on a local scale, i.e. we have not linked our results to the global geologic water cycle—the outgassing of water at mid-ocean ridges and hotspots and the recycling of water into the mantle at subduction zones. We will next explore water recycling at subduction zones on a global scale by linking our modeling results to the global geologic water cycle.

We have shown that the average plate age and overturn rate, i.e. the style of mantle convection, may influence the amount of water that is re-injected into the mantle at subduction zones. The style of mantle convection has probably changed over geologic time with the average overturn rate decreasing and the average seafloor (plate) age increasing with time. One way to determine the Earth's average plate age and overturn rate through time is to use a parameterized mantle convection model. Phipps Morgan [43] proposed one possible parameterization and argued that if the Earth's mantle temperature has remained fairly constant over time, then the amount of radiogenic heat production has to be equal to the degree of convective cooling. This assumption yields the conclusion that the mantle overturn rate, R, is proportional to the square of radiogenic heating, Q, so that $R \sim Q^2$. Likewise the average seafloor age A will be inversely proportional to Q^2, i.e. $A \sim 1/Q^2$. These considerations suggest that the average slab age and speed evolved over geologic time as shown in Fig. 8.

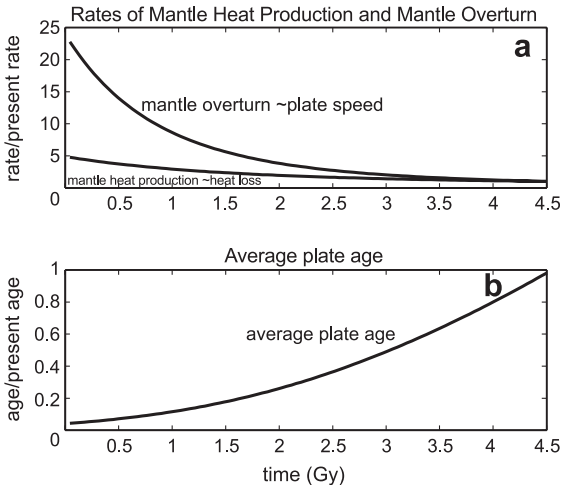

Fig. 8. Possible evolution of the mantle's average overturn rate (a) and ocean floor's average age (b). Estimates are based on the assumption that the overturn rate is proportional to the square of radioactive heat production.

In (a) it is seen that the mantle differentiation rate and thereby the average plate speed has experienced a 25-fold decrease while the average plate age has increased by a factor of ~25 over time (b). Note that these implications may be significantly different if the Earth's mantle temperature has strongly changed over geologic time; the argument that it remained constant (or cooled by less than 300 °C) is based on komatiite data and Phipps Morgan gives a more thorough explanation—see [44] for a review of komatiites and the thermal evolution of the Earth.

We use these values to parameterize water retention in subducting plates as a function of Earth age. We do this by running a series of models assuming the different plate ages and speeds provided by the parameterized mantle convection model. To the outcome of these model runs (Table 2) we fit a function that thereby provides slab water retention as a function of time since accretion, $H_2O_{ret}(t)$. We can now deduce equations for water outgassing and water recycling as a function of time:

$$H_2O_{out}(t) = \frac{R(t)}{R_0} P_0 f_{H_2O} H_2O_{mantle}(t) \quad (11)$$

$$H_2O_{in}(t) = \frac{R(t)}{R_0} S_0 H_2O_{ret}(t). \quad (12)$$

Here P_0 is the ridge differentiation rate that describes the fraction of mantle that is currently 'processed' at mid-ocean ridges and hotspots per time; it is deduced from the present-day overturn rate of the mantle $R_0 = 9.5$ Ga. The term f_{H_2O} is set to 0.99 and describes the degree of volatile loss during melting and $H_2O_{mantle}(t)$ is the changing water content of the mantle, and S_0 is the average present-day spreading rate 2.7 km^2/year. Note that the above equations imply that the total trench length remained constant through time.

Table 2
Water retention in a column of subducting slab as a function of the Earth's age

Time since accretion (Ga)	Total water retained	Sediments	Crust	5% Serp. mantle
0.5	0.21	0.07	0.14	0.0
1.0	0.23	0.09	0.14	0.0
1.5	0.26	0.12	0.14	0.0
2.0	0.28	0.14	0.14	0.0
2.5	0.46	0.15	0.14	0.17
3.0	0.8	0.16	0.16	0.48
3.5	1.0	0.17	0.17	0.7
4.0	1.24	0.17	0.19	0.87
4.5	1.59	0.18	0.3	1.1

All values for water retention are given in 10^5 kg/m^2.

Solving these equations yields an evolution curve for water in the mantle and exosphere over geologic time. To make this value more comparable to geologic observations, we use a simple model to transform changes in the exosphere's water to sea level changes. This model is based on the assumption that the global area occupied by oceans (A_{oceans}) and continents, respectively, has remained constant over time. However, the average seafloor age has changed with time and we do account for changes in ocean depth (d) with seafloor age. Changes in ocean depth due to thermal subsidence can be written as:

$$d_{past} = 2500(\mathrm{m}) + 233\left(\frac{\mathrm{m}}{\sqrt{\mathrm{Ma}}}\right)\sqrt{\tau(\mathrm{Ma})} \quad (13)$$

$$d_{now} = 2500(\mathrm{m}) + 233\left(\frac{\mathrm{m}}{\sqrt{\mathrm{Ma}}}\right)\sqrt{100(\mathrm{Ma})}; \quad (14)$$

and the present-day (V_{now}) and past (V_{past}) volumes of water in the exosphere are:

$$V_{now} = (d_{now} + 0)A_{oceans} => A_{oceans} = \frac{V_{now}}{d_{now}} \quad (15)$$

$$V_{past} = (d_{past} + h_{past})A_{oceans}. \quad (16)$$

In this scenario, sea level changes, h, over geologic time can be written as:

$$h_{past} = \frac{V_{past}}{V_{now}} d_{now} - d_{past} \quad (17)$$

In this formulation, sea level changes are only due to exosphere water volume and mean seafloor depths variations through time—other factors like glaciation are not accounted for.

We iteratively choose for each model the starting conditions, so that the present-day value of water in

the exosphere (cont. crust plus oceans) of 2.2×10^{21} kg [45] is reproduced. We further initialize all model runs by assuming that 95% of the initial water is in the mantle at time zero. Fig. 9 shows two typical evolution scenarios: a,b show a model run assuming 5% sub-Moho serpentinization and c,d show an evolution scenario that does not include water in the slab mantle. The solid lines in the upper panel plots (a,c) show water in the exosphere and the dashed-dotted line water in the mantle. We have further plotted the exosphere's ^{36}Ar fraction (normalized to the initial mantle value) as a reference curve for mantle degassing (dotted line). We assume that degassed mantle ^{36}Ar is not recycled back into the mantle but remains entirely in the exosphere, so that the exosphere's ^{36}Ar content is a measure for the degree of 'primordial' mantle degassing.

In b,d the water outgassing rate, the total water recycling rate at subduction zones, and the recycling rate in serpentinized mantle are plotted. To lose its much higher early heat production, mantle differentiation rates were much higher early on in Earth history; this resulted in much higher water outgassing rates. These outgassing rates were higher than the recycling rates at subduction zones (where young seafloor was being recycled), so that the exosphere's free water content increased and the mantle's water content decreased. In the model run that includes

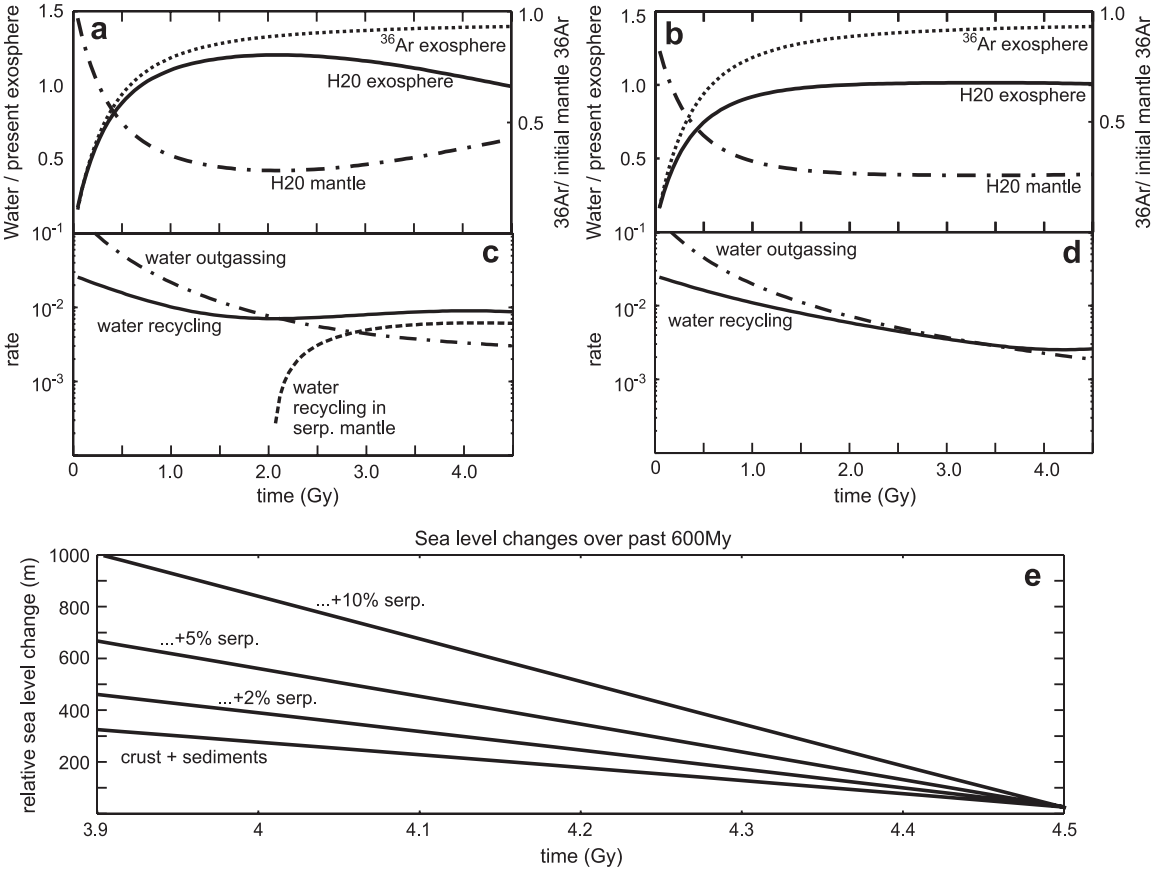

Fig. 9. The geologic water cycle. In (a,b) the water content of the Earth's mantle and exosphere is plotted against time along with the exosphere's ^{36}Ar content for two example model runs assuming 5% sub-Moho serpentinization (a) and no serpentinization (b); (c,d) show water recycling rates at subduction zones and the water outgassing rates at ridges and hotspots over time; (e) shows predicted sea level changes over the past 600 Ma for four different model runs assuming different initial plate hydrations (degree of near Moho serpentinization). See text for modeling details.

serpentine, after ~2.0 Ga subduction becomes sufficiently cold for serpentine to transform to higher pressure hydrous 'phase A' and water recycling at subduction zones starts to dominate, so that the exosphere's water fraction decreases again. These conditions persist up to the present, resulting in a predicted continuous drop in exosphere water over the past ~2.25 Ga. Present-day conditions are characterized by 0.49 'exospheres' of water in the mantle. In the model run that neglects serpentine as a water source (b,d), water recycling at subduction zone dominates over water outgassing only for the last 1 Ga. This scenario results in 0.38 'exospheres' of water in the present-day mantle.

We have made a series of model runs assuming different degrees of sub-Moho serpentinization (0–10%). The outcomes of these model runs are summarized in Table 3: the present-day mantle has highly outgassed (93%) and contains only between 28% and 47% of its initial water content. Present-day mantle water is therefore in all model runs mostly recycled water from the exosphere. Inferred initial water contents of the Earth's mantle vary between 1.4 (0% serpentine) and 1.9 (10% serpentine) present-day 'exospheres' of water.

In Fig. 9e we show predicted sea level changes over the past 600 Ma. We only show sea level changes for the last 600 Ma because only for this age range good geologic data is available. Hallam [46] estimated a maximum sea level drop of ~500 m over the past 600 Ma. These estimates are consistent with less than ~5% sub-Moho mantle serpentinization. Higher degrees of serpentinization seem to lead to too strong water recycling into the mantle to be consistent with global sea level changes since the Cambrian. In fact, even small degrees of serpentinization may have a big effect on sea level: 2% sub-Moho serpentinization causes a sea level change of ~150 m over the past 600 Ma. However, when serpentine is neglected as a fluid host, subduction-associated recycling of water in sediments and crust nonetheless influences the exosphere's water content. We find a 320-m sea level drop over the past 600 Ma for the 'no-serpentine' model run.

Table 3
Model parameters used for the parameterized convection calculations

Mantle serp. (%)	Initial H_2O	Present H_2O mantle	Mantle H_2O loss (%)	Outgassing (%)
0	1.4	0.39	72	93
2	1.5	0.49	67	93
5	1.63	0.64	61	93
10	1.88	0.89	53	93

Initial water and present-day water contents are in present-day 'exospheres'. In all model runs, the present-day water content in the exosphere is 1. See text for details.

The above calculated water cycles have significant implications for the geodynamic evolution of the Earth. Depending on the degree of serpentinization, peak sea level conditions were reached between ~2.5 Ga (10% serp.) and ~900 Ma (0% serp.) ago. Also the relative change in exosphere water volume between peak sea level and present-day conditions is strongly dependent on the amount of recycled water (i.e. the degree sub-Moho serpentinization): we find that for the four model runs (0%, 2%, 5%, 10% serpentinization) the relative changes in exosphere water volume between peak sea level conditions and today are 1%, 8%, 18%, and 31%, respectively. This implies that the more water is reinjected into the mantle at subduction zones, the earlier in Earth history peak sea level conditions were reached, and the higher was the change in free water volume between peak sea level and present-day conditions.

Furthermore, the predicted geologic water cycle suggests strong water loss from the mantle into the exosphere, so that the present-day mantle contains only 'little' water that is mostly recycled water. This contradicts somewhat the results of some earlier studies that pointed out the potential existence of several 'oceans' of primordial water in the Earth's lower mantle and transition zone, e.g. [47]. Part of this contradiction can be explained by the implicit pattern of mantle flow assumed in this study: we assume whole mantle flow, so that eventually the 93% of the mantle participates in near-surface upwelling, melting, and differentiation processes. The details of this mantle flow model are described in [48]. If a strictly layered Earth is assumed to have always existed, it is possible that a reservoir of incommunicative 'primitive' mantle water would still not yet have 'participated' in the surface geologic water cycle. However, for the reasons summarized in [48], we still believe that strongly layered mantle convection is improbable. Furthermore, in this scenario water in the 'communicative' regions of the mantle will be dominated by recycled water.

6. Conclusions

We have formulated a two-dimensional thermodynamical model that solves for the temperature and mantle flow within a subduction zone. Additionally, we have presented a tracer-based model to solve for slab fluid release. Using this model, we have explored how slabs dewater during subduction and how water cycling at convergent margins may be related to the geologic water cycle. Several conclusions can be drawn from these calculations:

(1) Slabs seem to dewater continuously during subduction. However, the 'host' lithology of the released fluids changes with depth: first, sediments dewater at shallow levels, second the altered ocean crust releases its water, and finally the hydrated lithospheric mantle deserpentinizes. This change in fluid source with depth may have strong implications for element recycling beneath arcs.
(2) Serpentinized mantle seems to be the best, i.e. most stable, lithology to transfer chemically bound water through the sub-arc dewatering region to greater mantle depths. Depending on the thermal structure of the subducting slab, up to 40% of the water stored in serpentinized mantle may be transferred into the deeper mantle.
(3) The Earth mantle is likely to have lost most of its initial water (53–78%) to exhale the oceans. Present-day mantle water is mostly recycled water from the exosphere. Since ~ 2–2.5 Ga, when subduction became sufficiently cold, this water recycling may be dominated by serpentinized mantle even if small degrees of serpentinization are assumed.

Acknowledgements

This paper benefited from thorough and helpful reviews by Paul Tackley and an anonymous reviewer. Many thanks also to Stefano Poli and Patrizia Fumagalli for interesting and fruitful discussions. Sonderforschungsbereich 574 'Volatiles and fluids in subduction zones' at Kiel University contribution 59. ***[EB]***

References

[1] S.M. Peacock, Are the lower planes of double seismic zones caused by serpentine dehydration in subducting oceanic mantle? Geology 29 (2001) 299–302.
[2] L.H. Rüpke, J. Phipps Morgan, M. Hort, J.A.D. Connolly, Are the regional variations in Central American arc lavas due to differing basaltic versus peridotitic slab sources of fluids? Geology 30 (2002) 1035–1038.
[3] C.R. Ranero, J. Phipps Morgan, K.D. McIntosh, C. Reichert, Bending, faulting, and mantle serpentinization at the Middle America trench, Nature 425 (2003) 367–373.
[4] D.M. Kerrick, Serpentinite seduction, Science 298 (2002) 1344–1345.
[5] T. Elliot, T. Plank, A. Zindler, W. White, B. Bourdon, Element transport from slab to volcanic front at the Mariana arc, Journal of Geophysical Research 102 (1997) 14991–15019.
[6] A.W. Hofmann, Mantle geochemistry: the message from oceanic volcanism, Nature 385 (1997) 219–229.
[7] R.M. Canup, K. Righter, Origin of the Earth and Moon, University of Arizona Press, Tucson, AZ, 2000.
[8] T. Plank, H. Langmuir, The chemical composition of subducting sediment and its consequences for the crust and mantle, Chemical Geology 145 (1998) 325–394.
[9] H. Staudigel, T. Plank, B. White, H.-U. Schmincke, Geochemical fluxes during seafloor alteration of the basaltic upper ocean crust: DSDP sites 417 and 418, in: G.E. Bebout, D.W. Scholl, S.H. Kirby, J.P. Platt (Eds.), Subduction Top to Bottom, American Geophysical Union, Washington, DC, 1996, pp. 19–38.
[10] D.M. Kerrick, J.A.D. Connolly, Metamorphic devolotilization of subducted marine sediments and the transport of volatiles into the Earth's mantle, Nature 411 (2001) 293–296.
[11] K. Wallmann, The geological water cycle and the volution of marine d18O values, Geochimica et Cosmochimica Acta 65 (2001) 2469–2485.
[12] M.W. Schmidt, S. Poli, Experimentally based water budgets for dehydrating slabs and consequences for arc magma generation, Earth and Planetary Science Letters 163 (1998) 361–379.
[13] P. Ulmer, V. Trommsdorf, Serpentine stability to mantle depths and subduction-related magmatism, Science 268 (1995) 858–861.
[14] T. Seno, Y. Yamanaka, Double seismic zones, compressional deep trench-outer rise events, and superplumes, in: G.E. Bebout, D.W. Scholl, S.H. Kirby, J.P. Platt (Eds.), Subduction: Top to Bottom, AGU, Washington, DC, 1996.
[15] D.P. Dobson, P.G. Meredith, S.A. Boon, Simulation of subduction zone seismicity by dehydration of serpentine, Science 298 (2002) 1407–1410.
[16] S. Kirby, E.R. Engdahl, R. Denlinger, Intermediate-depth intraslab earthquakes and arc volcanism as physical expressions of crustal and uppermost mantle metamorphism in subducting slabs, in: G.E. Bebout, D.W. Scholl, S.H. Kirby, J.P. Platt (Eds.), Subduction: Top to Bottom, American Geophysical Union, Washington, DC, 1996, pp. 195–214.
[17] T. John, V. Schenk, Partial eclogitisation of gabbroic rocks in

a late Precambrian subduction zone (Zambia): prograde metamorphism triggered by fluid infiltration, Contributions to Mineralogy and Petrology 146 (2003) 174–192.
[18] A. Berhorst, E.R. Flueh, K.D. McIntosh, C.R. Ranero, I. Ahmed, E.A. Silver, U. Barckhausen, The crustal structure of the convergent Nicaraguan margin from a combined reflection and refraction study, Geophysical Research Abstracts 5 (2003) 09692.
[19] V. Sallares, C.R. Ranero, Structure of the incoming ocean plate and the erosional convergent margin off Antofagasta, northern Chile, Geophysical Research Abstracts 5 (2003) 02839.
[20] J.H. Davies, D.J. Stevenson, Physical model of source region of subduction zone volcanics, Journal of Geophysical Research 97 (1992) 2037–2070.
[21] S.M. Peacock, Thermal and petrological structure of subduction zones, in: G.E. Bebout, D.W. Scholl, S.H. Kirby, J.P. Platt (Eds.), Subduction: Top to Bottom, American Geophysical Union, 1996.
[22] S.M. Peacock, K. Wang, Seismic consequences of warm versus cool subduction metamorphism: examples from southwest and northeast Japan, Science 286 (1999) 937–939.
[23] C. Kincaid, I.S. Sacks, Thermal and dynamical evolution of the upper mantle in subduction zones, Journal of Geophysical Research 102 (1997) 12295–12315.
[24] J. van Hunen, A.P. van den Berg, N.J. Vlaar, A thermo-mechanical model of horizontal subduction below an overriding plate, Earth and Planetary Science Letters 182 (2000) 157–169.
[25] F. Funiciello, G. Morra, K. Regenauer-Lieb, D. Giardini, Dynamics of retreating slabs: 1. Insights from two-dimensional numerical experiments, Journal of Geophysical Research 108 (2003) DOI:10.1029/2001JB000898.
[26] P.E. van Keken, B. Kiefer, S.M. Peacock, High-resolution models of subduction zones: implications for mineral dehydration reactions and the transport of water into the deep mantle, Geochemistry Geophysics Geosystems 3 (2002) ISI: 000178769500001.
[27] T. Gerya, D. Yuen, Rayleigh–Taylor instabilities from hydration and melting propel 'cold plumes' at subduction zones, Earth and Planetary Science Letters 212 (2003) 47–62.
[28] B.R. Hacker, G.A. Aber, S.M. Peacock, Subduction factory: 1. Theorectical mineralogy, densities, seismic wave speeds, and H20 contents, Journal of Geophysical Research 108 (2003) 2029 DOI:10.1029/2001JB001127.
[29] B.R. Hacker, S.M. Peacock, G.A. Aber, D. Holloway, Subduction factory 2. Are intermediate-depth earthquakes in subducting slabs linked to metamorphic dehydration reactions? Journal of Geophysical Research 108 (2003) DOI:10.1029/2001JB001129.
[30] C. Dumoulin, M.-P. Doin, L. Fleitout, Heat transport in stagnant lid convection with temperature- and pressure-dependent Newtonian or non-Newtonian rheology, Journal of Geophysical Research 104 (1999) 12759–12777.
[31] P.K. Smolarkiewicz, A fully multidimensional positive definite advection transport algorithm with small implicit diffusion, Journal of Computational Physics 54 (1984) 325–362.
[32] J.S. Brock, J.W. Painter, D.B. Kothe, Tracer–Particle Advection: Algorithm Components and Implementation Methods, Los Alamos National Laboratory Reports, 1998.
[33] J.A.D. Connolly, K. Petrini, An automated strategy for calculation of phase diagram sections and retrieval of rock properties as a function of physical conditions, Journal of Metamorphic Geology 20 (2002) 697–708.
[34] A.H.E. Roehm, R. Snieder, S. Goes, J. Trampert, Thermal structure of continental upper mantle inferred from S-wave velocity and surface heat flow, Earth and Planetary Science Letters 181 (2000) 395–407.
[35] D.M. Kerrick, J.A.D. Connolly, Metamorphic devolatilization of subducted oceanic metabasalts: implications for seismicity, arc magmatism and volatile recycling, Earth and Planetary Science Letters 189 (2001) 19–29.
[36] R.J. Angel, D.J. Frost, N.L. Ross, R. Hemley, Stabilities and equation of state of dense hydrous magnesium silicates, Physics of the Earth and Planetary Interiors 127 (2001) 181–196.
[37] S. Poli, M.W. Schmidt, Petrology of subducted slabs, Annual Review of Earth and Planetary Sciences 30 (2002) 207–235.
[38] K. Bose, A. Navrotsky, Thermochemistry and phase equilibria of hydrous phases in the system $MgO–SiO_2–H_2O$: implications for volatile transport to the mantle, Journal of Geophysical Research 103 (1998) 9713–9719.
[39] A.B. Thompson, Water in the Earth's upper mantle, Nature 358 (1992) 295–302.
[40] R.W. Luth, Is phase a relevant to the Earth's mantle? Geochimica et Cosmochimica Acta 59 (1995) 679–682.
[41] A.R. Pawley, B.J. Wood, The low-pressure stability of phase A; Mg7Si2O8(OH)6, Contributions to Mineralogy and Petrology 124 (1996) 90–97.
[42] T.J.B.H. Holland, R. Powell, An internally consistent thermodynamic data set for phases of petrologic interest, Journal of Metamorphic Geology 16 (1998) 309–343.
[43] J. Phipps Morgan, Thermal and rare gas evolution of the mantle, Chemical Geology 145 (1998) 431–445.
[44] T.L. Grove, S.W. Parman, Thermal evolution of the Earth as recorded by komatiites, Earth and Planetary Science Letters 219 (2004) 173–187.
[45] P. Henderson, Inorganic Geochemistry, Pergamon, Oxford, 1986.
[46] A. Hallam, Phanerozoic Sea-Level Changes, Columbia University Press, New York, 1992.
[47] M. Murakami, K. Hirose, H. Yurimoto, S. Nakashima, N. Takafuji, Water in Earth's Lower Mantle, Science 295 (2002) 1885–1887.
[48] J. Phipps Morgan, J. Morgan, Two-stage melting and the geochemical evolution of the mantle: a recipe for mantle plum-pudding, Earth and Planetary Science Letters 170 (1999) 215–239.
[49] C. Hensen, K. Wallmann, M. Schmidt, C. Ranero, E. Suess, Fluid expulsion related to mud extrusion off Costa Rica: a window to the subducting slab, Geology 32 (2004) 201–204.
[50] T.V. Gerya, B. Stockhert, A.L. Perchuk, Exhumation of high-pressure metamorphic rocks in a subduction channel: a numerical simulation, Tectonics 21 (2002) DOI:10.1029/2002TC001406.